

# Fluctuation and interaction induced instability of dark solitons in single and binary condensates

Arko Roy and D. Angom

*Physical Research Laboratory, Navrangpura, Ahmedabad-380009, Gujarat, India*

We show that the presence of soliton in a single-species condensate, at zero temperature, enhances the quantum depletion sufficient enough to induce dynamical instability of the system. We also predict that for two-species condensates, two Goldstone modes emerge in the excitation spectrum at phase separation. Of these, one is due to the presence of the soliton. We use Hartree-Fock-Bogoliubov theory with Popov approximation to examine the mode evolution, and demonstrate that when the anomalous mode collides with a higher energy mode it renders the solitonic state oscillatory unstable. We also report soliton induced change in the topology of the density profiles of the two-species condensates at phase-separation.

PACS numbers: 03.75.Mn, 03.75.Hh, 67.85.Bc

## I. INTRODUCTION

The experimental realization of single and multi-component Bose-Einstein condensates (BECs) in atomic gases have opened up the possibility of exploring topological defects. Due to the ubiquitous presence of topological defects in nature, study of matter-wave excitations such as vortices and solitons in atomic BECs has been a topic of extensive research both experimentally and theoretically over the last few years. In fact, these have attracted much attention as they are created spontaneously during BEC phase transition through Kibble-Zurek mechanism [1–4]. A soliton, for instance can be used to probe the phase of the image acquired in a BEC interferometer as proposed by Negretti *et. al* [5, 6]. These and other novel phenomena have inspired numerous experiments [7, 8] and theoretical studies [9–15] with dark and bright solitons in atomic BECs in a wide range of settings under different scenarios. The experimental observation shows that the notch of the dark soliton gets filled up with thermal atoms over time and the soliton becomes gray, hence starts oscillating which are either short- or long-lived depending upon the system of interest [16–18].

On the theoretical front, most of the studies on the statics and the dynamics of dark solitons have been carried out in quasi-1D setting at zero temperature where thermal fluctuations can be ignored [19]. There have been several works on stability of solitons in cigar-shaped double well potential [20], disordered potential [21], and optical lattice [22–25]. Stability of multiple solitons in quasi-1D trap has also been examined [26, 27]. Quantum depletion in BECs with soliton at  $T = 0$  in weakly interacting Bose gases has also been studied using approximate models [28–34]. This motivated us to reexamine the role of quantum fluctuations in BECs, whether it be with or without soliton. We show that quantum fluctuation in BECs with soliton is higher than without it. This is due to the presence of the anomalous mode, and we demonstrate that quantum fluctuations can make the dark soliton gray, which as a result becomes dynamically unstable.

The two-component BECs (TBECs), on the other have different ground states depending on the interactions, as compared to a single-component BEC. The most unique aspect of TBECs is the phenomenon of phase separation. Most importantly, in experiments, the TBEC can be steered from miscible to phase-separated domain or vice versa through a Feshbach resonance [35, 36]. This has motivated numerous theoretical investigations on stationary states [37–39], dynamical instabilities [40–42], and collective excitations [43–47] of TBEC. Furthermore, repulsive TBECs support coupled dark-bright solitons which makes it richer and more interesting than single-component BECs [10]. The bright soliton, on the other hand, cannot survive in single component BECs with repulsive interaction. It may be mentioned here that, solitons in BECs and TBECs have been experimentally achieved either by phase-imprinting method [16] or in two counter-flowing miscible TBECs above a critical velocity [48]. For miscible TBECs, creation and interaction of dark solitons has been theoretically examined in Refs. [49, 50]. Families of stable solitonic solutions from coupled Gross-Pitaevskii (GP) equations in quasi-1D TBECs at zero temperature have been obtained [51, 52].

In the present work, we describe the development of Hartree-Fock-Bogoliubov theory with Popov (HFB-Popov) approximation for trapped TBECs. We use it to examine the evolution of Goldstone modes and mode energies for TBEC with soliton as a function of interspecies scattering length. Recent works [43–46] have reported the existence of an additional Goldstone mode at phase separation in the symmetry-broken density profiles. We have demonstrated in our earlier work [45] that in the *sandwich type* density profiles where one of the species is surrounded on both sides by the other, the mode evolves very differently with the appearance of a third Goldstone mode. In the present work, we show the presence of the soliton introduces an additional Goldstone mode to the system. Even at zero temperature without considering any quantum fluctuation, for certain range of interspecies scattering length, the TBEC becomes dynamically unsta-

ble. The difference in the mass of the two species also plays a significant role in mode evolution and topology of density profiles.

## II. THEORY

### A. Single component BEC

For a quasi-1D system, the trapping frequencies in  $V = (1/2)m(\omega_x^2 x^2 + \omega_y^2 y^2 + \omega_z^2 z^2)$  should satisfy the condition  $\omega_x = \omega_y = \omega_\perp \gg \omega_z$ . The condensate wave function in such a potential can be integrated out along  $xy$  direction to reduce it to a quasi-1D system. The grand-canonical Hamiltonian, in second quantized form, describing an interacting BEC is then

$$H = \int dz \hat{\Psi}^\dagger(z, t) \left[ -\frac{\hbar^2}{2m} \frac{\partial^2}{\partial z^2} + V(z) - \mu \right. \\ \left. + \frac{U}{2} \hat{\Psi}^\dagger(z, t) \hat{\Psi}(z, t) \right] \hat{\Psi}(z, t), \quad (1)$$

where  $\hat{\Psi}$  is the Bose field operator of the single species BEC, and  $\mu$  is the chemical potential. The strength of the intra-species repulsive interactions is  $U = (a\lambda)/m$ , where  $\lambda = (\omega_\perp/\omega_z) \gg 1$  is the anisotropy parameter,  $a$  is the  $s$ -wave scattering length,  $m$  is the atomic mass of the species. Starting with this Hamiltonian, the equation of motion of the Bose field operator is

$$i\hbar \frac{\partial}{\partial t} \hat{\Psi} = \hat{h} \hat{\Psi} + U \hat{\Psi}^\dagger \hat{\Psi} \hat{\Psi}, \quad (2)$$

where  $\hat{h} = (-\hbar^2/2m)\partial^2/\partial z^2 + V(z) - \mu$ . For the sake of simplicity of notation, we will refrain from writing the explicit dependence of  $\hat{\Psi}$  on  $z$  and  $t$ . Since a majority of the atoms populate the ground state for the temperature domain pertinent to the experiments ( $T \leq 0.65T_c$ ) [53], the condensate part can be separated out from the Bose field operator  $\hat{\Psi}(z, t)$ . The non-condensed or the thermal cloud of atoms are then the fluctuations of the condensate field. Here,  $T_c$  is the critical temperature of ideal gas in a harmonic confining potential. Accordingly, we define [54],  $\hat{\Psi}(z, t) = \phi(z, t) + \tilde{\psi}(z, t)$ , where  $\phi(z, t)$  is a  $c$ -field and represents the condensate, and  $\tilde{\psi}(z, t)$  is the fluctuation part. For a single component BEC,  $\hat{\Psi}$  can then be written as

$$\hat{\Psi} = \phi + \tilde{\psi}. \quad (3)$$

Thus for a single-species BEC, the equation of motion of the condensate within the time-independent HFB-Popov approximation is given by the generalized GP equation

$$\hat{h}\phi + U[n_c + 2\tilde{n}]\phi = 0. \quad (4)$$

In the above equation,  $n_c(z) \equiv |\phi(z)|^2$ ,  $\tilde{n}(z) \equiv \langle \tilde{\psi}^\dagger(z, t) \tilde{\psi}(z, t) \rangle$ , and  $n(z) = n_c(z) + \tilde{n}(z)$  are the local

condensate, non-condensate, and total density, respectively. Using Bogoliubov transformation, the fluctuations are

$$\tilde{\psi}(z, t) = \sum_j \left[ u_j(z) \hat{\alpha}_j(z) e^{-iE_j t} - v_j^*(z) \hat{\alpha}_j^\dagger(z) e^{iE_j t} \right], \\ \tilde{\psi}^\dagger(z, t) = \sum_j \left[ u_j^*(z) \hat{\alpha}_j^\dagger(z) e^{iE_j t} - v_j(z) \hat{\alpha}_j(z) e^{-iE_j t} \right].$$

Here,  $\hat{\alpha}_j$  ( $\hat{\alpha}_j^\dagger$ ) are the quasiparticle annihilation (creation) operators and satisfy the usual Bose commutation relations, and the subscript  $j$  represents the energy eigenvalue index. From the above definitions, we get the following Bogoliubov-de Gennes (BdG) equations

$$(\hat{h} + 2Un)u_j - U\phi^2 v_j = E_j u_j, \quad (5a)$$

$$-(\hat{h} + 2Un)v_j + U\phi^{*2} u_j = E_j v_j. \quad (5b)$$

The number density  $\tilde{n}$  of non-condensate particles is then

$$\tilde{n} = \sum_j \{ [|u_j|^2 + |v_j|^2] N_0(E_j) + |v_j|^2 \}, \quad (6)$$

where  $\langle \hat{\alpha}_j^\dagger \hat{\alpha}_j \rangle = (e^{\beta E_j} - 1)^{-1} \equiv N_0(E_j)$  with  $\beta = 1/k_B T$ , is the Bose factor of the quasi-particle state with energy  $E_j$  at temperature  $T$ . However, it should be emphasized that, when  $T \rightarrow 0$ ,  $N_0(E_j)$ 's in Eq. (6) vanishes. The non-condensate density is then reduced to

$$\tilde{n} = \sum_j |v_j|^2. \quad (7)$$

Thus, at zero temperature we need to solve the equations self-consistently as the quantum depletion term  $|v_j|^2$  in the above equation is non-zero.

### B. Harmonic oscillator basis

We solve the quasi-particle amplitudes  $u_j, v_j$ 's in the basis of the harmonic oscillator trapping potential.

$$u_j = \sum_{i=0}^{N_b} p_{ij} \xi_i, \quad v_j = \sum_{i=0}^{N_b} q_{ij} \xi_i, \quad (8)$$

where  $\xi_i$  is the  $i$ th harmonic oscillator eigenstate and  $N_b$  is the number of basis that is considered. Using this expansion, Eq. (5) is then reduced to a matrix eigenvalue equation and solved using standard matrix diagonalization algorithms. The matrix has a dimension of  $2N_b \times 2N_b$ , and is non-Hermitian, non-symmetric and may have complex eigenvalues. The eigenvalue spectrum obtained from the diagonalization of the matrix has an equal number of positive and negative eigenvalues  $E_j$ 's. In addition, the amount of energy that is carried by the eigenmode  $j$  is given by

$$\Delta_j = \int dz (|u_j|^2 - |v_j|^2) E_j. \quad (9)$$

The sign of the quantity  $\Delta_j$  is known as *Krein sign*. If this sign turns out to be negative for a mode  $j$ , then the corresponding mode is called as the *anomalous mode*. It signifies the energetic instability which may be present due to a topological defect in the system.

### C. Hartree-Fock basis

To incorporate the interactions present in the system while calculating the Bogoliubov quasi-particle amplitudes  $u_j$  and  $v_j$ 's more efficiently, in terms of basis size, we resort to Hartree-Fock basis. Thus, to solve Eq. (5), we define  $u_j$ 's and  $v_j$ 's as a linear combination of *Hartree-Fock basis* functions  $\zeta_k$ ,

$$u_j = \sum_k c_k^j \zeta_k, v_j = \sum_k d_k^j \zeta_k, \quad (10)$$

where  $c_k$ , and  $d_k$  are the coefficients of linear combination. In principle, the GP equation has an infinite number of eigenvalues  $\epsilon_k$  and eigenvectors  $\zeta_k$ . In general, Eq. (4) can then be recast into a matrix eigenvalue equation

$$\mathcal{H}\zeta_k = \epsilon_k \zeta_k, \quad (11)$$

where  $\mathcal{H} = \hat{h} + U[n_c + 2\tilde{n}]$ , and  $k$  stands for the eigenvalue index. The eigensolution with the lowest eigenvalue  $\epsilon_0$  is referred to as the condensate ground state with the condensate wave function  $\phi \equiv \zeta_0$ . To calculate the quasi-particle amplitudes  $u_j$ 's and  $v_j$ 's we again expand the eigensolutions  $\zeta_k$  in terms of  $\xi_i$ , then

$$\zeta_k = \sum_i a_i^k \xi_i, \quad (12)$$

Taking the orthogonality and linear independence of  $\xi_i$ s into account and plugging Eq. (12) in Eq. (11), one can obtain the expansion coefficients  $a_k$  used in decomposing the above equation. This yields a set of basis functions  $\{\zeta_k\}$ , which is generally referred to as the *Hartree-Fock basis*. The choice of  $\zeta_k$  reduces the number of basis functions required in the calculation of  $u_j$  and  $v_j$ 's as  $\zeta_k$  subsumes the effect of interactions in the system.

### D. Two component BEC

Similarly, for a TBEC in a quasi-1D trapped system,

$$\begin{aligned} H = \sum_{k=1,2} \int dz \hat{\Psi}_k^\dagger(z,t) & \left[ -\frac{\hbar^2}{2m_k} \frac{\partial^2}{\partial z^2} + V_k(z) - \mu_k \right. \\ & \left. + \frac{U_{kk}}{2} \hat{\Psi}_k^\dagger(z,t) \hat{\Psi}_k(z,t) \right] \hat{\Psi}_k(z,t) \\ & + U_{12} \int dz \hat{\Psi}_1^\dagger(z,t) \hat{\Psi}_2^\dagger(z,t) \hat{\Psi}_1(z,t) \hat{\Psi}_2(z,t), \quad (13) \end{aligned}$$

where  $k = 1, 2$  is the species index,  $\hat{\Psi}_k$ 's are the Bose field operators of the two different species, and  $\mu_k$ 's

are the chemical potentials. The strength of intra and inter-species repulsive interactions are  $U_{kk} = (a_{kk}\lambda)/m_k$  and  $U_{12} = (a_{12}\lambda)/(2m_{12})$ , respectively, where  $\lambda = (\omega_\perp/\omega_z) \gg 1$  is the anisotropy parameter,  $a_{kk}$  is the  $s$ -wave scattering length,  $m_k$ 's are the atomic masses of the species and  $m_{12} = m_1 m_2 / (m_1 + m_2)$ . Starting with this Hamiltonian, the equation of motion of the Bose field operators is

$$i\hbar \frac{\partial}{\partial t} \begin{pmatrix} \hat{\Psi}_1 \\ \hat{\Psi}_2 \end{pmatrix} = \begin{pmatrix} \hat{h}_1 + U_{11} \hat{\Psi}_1^\dagger \hat{\Psi}_1 & U_{12} \hat{\Psi}_2^\dagger \hat{\Psi}_1 \\ U_{12} \hat{\Psi}_1^\dagger \hat{\Psi}_2 & \hat{h}_2 + U_{22} \hat{\Psi}_2^\dagger \hat{\Psi}_2 \end{pmatrix} \begin{pmatrix} \hat{\Psi}_1 \\ \hat{\Psi}_2 \end{pmatrix},$$

where  $\hat{h}_k = (-\hbar^2/2m_k)\partial^2/\partial z^2 + V_k(z) - \mu_k$ . In the same way as in single species case, we define [54],  $\hat{\Psi}(z,t) = \Phi(z) + \tilde{\Psi}(z,t)$ , where  $\Phi(z)$  is a  $c$ -field and represents the condensate, and  $\tilde{\Psi}(z,t)$  is the fluctuation part. In two component representation

$$\begin{pmatrix} \hat{\Psi}_1 \\ \hat{\Psi}_2 \end{pmatrix} = \begin{pmatrix} \phi_1 \\ \phi_2 \end{pmatrix} + \begin{pmatrix} \tilde{\psi}_1 \\ \tilde{\psi}_2 \end{pmatrix}, \quad (14)$$

where  $\phi_k(z)$  and  $\tilde{\psi}_k(z)$  are the condensate and fluctuation part of the  $k$ th species. Thus for a TBEC,  $\phi_k$ s are the stationary solutions of the coupled generalized GP equations, with time-independent HFB-Popov approximation, given by

$$\hat{h}_1 \phi_1 + U_{11} [n_{c1} + 2\tilde{n}_1] \phi_1 + U_{12} n_2 \phi_1 = 0, \quad (15a)$$

$$\hat{h}_2 \phi_2 + U_{22} [n_{c2} + 2\tilde{n}_2] \phi_2 + U_{12} n_1 \phi_2 = 0. \quad (15b)$$

In the above equation,  $n_{ck}(z) \equiv |\phi_k(z)|^2$ ,  $\tilde{n}_k(z) \equiv \langle \tilde{\psi}_k^\dagger(z,t) \tilde{\psi}_k(z,t) \rangle$ , and  $n_k(z) = n_{ck}(z) + \tilde{n}_k(z)$  are the local condensate, non-condensate, and total density, respectively. Using Bogoliubov transformation, the fluctuations are

$$\begin{aligned} \tilde{\psi}_k(z,t) &= \sum_j \left[ u_{kj}(z) \hat{\alpha}_j(z) e^{-iE_j t} - v_{kj}^*(z) \hat{\alpha}_j^\dagger(z) e^{iE_j t} \right], \\ \tilde{\psi}_k^\dagger(z,t) &= \sum_j \left[ u_{kj}^*(z) \hat{\alpha}_j^\dagger(z) e^{iE_j t} - v_{kj}(z) \hat{\alpha}_j(z) e^{-iE_j t} \right]. \end{aligned}$$

From this formalism we obtain the following BdG equations

$$\hat{\mathcal{L}}_1 u_{1j} - U_{11} \phi_1^2 v_{1j} + U_{12} \phi_1 (\phi_2^* u_{2j} - \phi_2 v_{2j}) = E_j u_{1j}, \quad (16a)$$

$$\hat{\mathcal{L}}_1 v_{1j} + U_{11} \phi_1^* u_{1j} - U_{12} \phi_1^* (\phi_2 v_{2j} - \phi_2^* u_{2j}) = E_j v_{1j}, \quad (16b)$$

$$\hat{\mathcal{L}}_2 u_{2j} - U_{22} \phi_2^2 v_{2j} + U_{12} \phi_2 (\phi_1^* u_{1j} - \phi_1 v_{1j}) = E_j u_{2j}, \quad (16c)$$

$$\hat{\mathcal{L}}_2 v_{2j} + U_{22} \phi_2^* u_{2j} - U_{12} \phi_2^* (\phi_1 v_{1j} - \phi_1^* u_{1j}) = E_j v_{2j}, \quad (16d)$$

where  $\hat{\mathcal{L}}_1 = (\hat{h}_1 + 2U_{11}n_1 + U_{12}n_2)$ ,  $\hat{\mathcal{L}}_2 = (\hat{h}_2 + 2U_{22}n_2 + U_{12}n_1)$  and  $\hat{\mathcal{L}}_k = -\hat{\mathcal{L}}_k$ . The number density  $\tilde{n}_k$  of non-condensate particles is then

$$\tilde{n}_k = \sum_j \{ |u_{kj}|^2 + |v_{kj}|^2 \} N_0(E_j) + |v_{kj}|^2, \quad (17)$$

To solve Eq. (16) we define  $u$  and  $v$ 's as linear combination of  $\xi_i$ s. The equation is then reduced to a matrix eigenvalue equation and solved using standard matrix diagonalization algorithms.

### III. THE DARK SOLITON

The location of a dark soliton is a place in a quasi-1D condensate is where the condensate wave function  $\phi(z)$  changes sign. The condensate wave function then has a kink where the density is zero. Typically, a wave function of the dark soliton is simply proportional to  $\tanh[(z - z_0)/\xi]$ , where  $\xi$  is a local value of the healing length at position  $z_0$  of the soliton. Hereafter, it is to be noted that the symbol  $\xi$  without any subscript refers to the healing length. Condensate with a soliton at  $z_0 = 0$  is an antisymmetric wave function of  $z$  and the phase of the wave function jumps discontinuously by  $\pi$  as  $z$  passes through zero. Even at  $T = 0$ , quantum depletion from the condensate leads to graying of the dark soliton. The kink of the soliton gets filled up with incoherent atoms quantum depleted from the condensate. The soliton is created by employing phase-imprinting method [16]. We assume that before phase imprinting all the atoms of the system is in symmetric ground state. Right after this operation one gets a condensate with an antisymmetric wave function.

## IV. RESULTS AND DISCUSSIONS

### A. Numerical Details

For single component BECs at  $T = 0$  studies we solve Eq. 4 neglecting the non-condensate density ( $\tilde{n} = 0$ ) using finite-difference methods and in particular, we use the split-step Crank-Nicholson method [55]. For TBECs, we proceed in a similar way by solving the pair of coupled Eqs. (15) and setting  $\tilde{n}_k = 0$ . The method when implemented with imaginary time propagation is appropriate to obtain the stationary ground state wave function of the single component BEC or TBEC. Furthermore, we use numerical implementation of the phase imprinting method to generate a dark soliton in (T)BEC. For this, we begin the simulation with imaginary time propagation of the GP equation and imprint  $\pi$  phase jump corresponding to a soliton at  $z_0 = 0$  by using  $\phi = |\phi| \exp(i\pi)$ . Using this solution of the GPE, and based on Eq. (8), we cast the Eq. (5) as a matrix eigenvalue equation in the basis of the trapping potential. The matrix is then diagonalized using the LAPACK routine `zgeev` [56] to find the quasi-particle energies and amplitudes,  $E_j$ , and  $u_j$ 's and  $v_j$ 's, respectively. We begin our  $T = 0$  calculations to account for quantum fluctuations with this step. This sets the starting point of the first iteration where the  $u_j$ 's and  $v_j$ 's along with positive energy modes  $E_j$ 's are used to get the initial estimate of  $\tilde{n}$  through Eq. (6). The ground state wave function  $\phi$  of BEC and chemical potential  $\mu$  are again re-determined from Eq. (4), using this updated value of  $\tilde{n}$ . For calculation of eigenmodes of TBEC with soliton, we again cast Eq. (16) as a matrix and diagonalize it [45]. During the calculation of the  $u_k$  and  $v_k$ , we choose an optimal number of the harmonic

oscillator basis functions.

### B. Single species BEC

The low-lying excitation spectrum of a quasi-1D BEC with a soliton is characterized by the presence of an anomalous mode, which indicates that the BEC is in an energetically excited state. This is in addition to the Goldstone and the Kohn modes, which are also present in the excitation spectrum of a quasi-1D BEC without soliton. The anomalous, and Kohn mode energies are real, and the energy of the anomalous mode  $\approx \hbar\omega_z/\sqrt{2}$ . A unique feature of the anomalous mode is the negative *Krein sign* [20, 28]. This shows the solitonic solution of the stationary quasi-1D GP equation is stable. However, when the solution is evolved in imaginary time, with the inclusion of  $\tilde{n}$  in the  $T = 0$  GP equation, the anomalous mode is transformed into an imaginary energy eigenmode. This is an unambiguous signature of quantum depletion induced instability of the solitonic solution. In other words, the non-zero  $\tilde{n}$  arising from the quantum fluctuations within the notch of the soliton turns it gray, and renders the system dynamically unstable. Furthermore, the low-lying energy spectrum is devoid of any negative *Krein sign* eigenmodes. The anomalous mode, however, reappears in the excitation spectrum on further evolving the system over imaginary time.

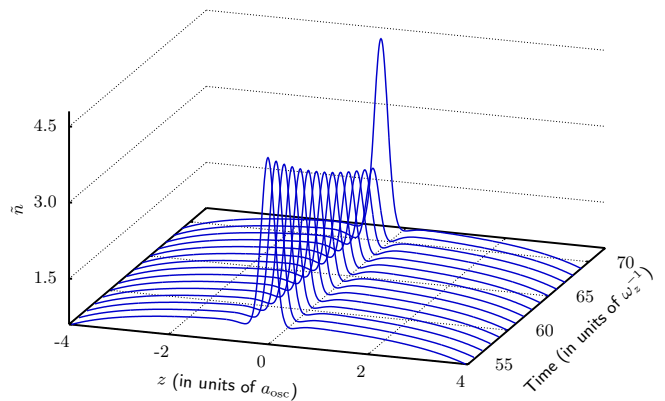


FIG. 1. The temporal evolution in the profile of the non-condensate atom density  $\tilde{n}$  at  $T = 0$  measured in units of  $a_{\text{osc}}^{-1}$ , where  $a_{\text{osc}} = \sqrt{\hbar/(m\omega_z)}$ . The plots show a steady drop in the number of non-condensate atoms till it reaches a threshold value, and then, the anomalous mode reappears in the spectrum. The latter is reflected in the profile of  $\tilde{n}$  at  $t = 69\omega_z^{-1}$ , where it has maximal distribution.

To further examine the trend in the evolution of  $E_{\text{an}}$ , the energy of the anomalous mode or the first excited state, we study the variation of  $\tilde{n}$  with time as shown in Fig. 1. The contribution from the anomalous mode fills up the notch of the soliton and  $\tilde{n}(0)$  has the largest possible value at the initial state of evolution. At later times,  $E_{\text{an}}$  is imaginary and  $\tilde{n}(0)$  decreases, the trend is

as shown in Fig. 1. However, when  $\tilde{n}(0)$  reaches a critical value, which in the present work is  $\approx 2.312 a_{\text{osc}}^{-1}$ , it is no longer large enough to render the solitonic solution unstable and the anomalous mode reappears. This confirms  $\tilde{n}(0)$  has a threshold value below which the solitonic solution may be stable.

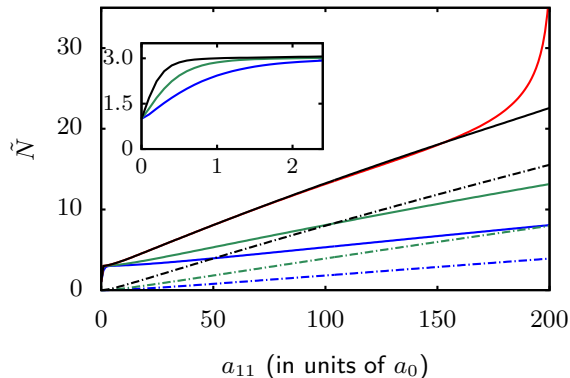


FIG. 2. Variation in the total number of non-condensate atoms  $\tilde{N}$  at  $T = 0$  as a function of the scattering length  $a_{11}$ . The solid (dashed) blue, green, and black lines represent  $\tilde{N}$  in the presence (absence) of soliton with total number of atoms  $N = 500, 1000$ , and  $2000$ , respectively. The solid red line represents  $\tilde{N}$  in the presence of soliton for  $N = 2000$ , with the number of basis  $N_b = 170$ , it is shown to indicate lack of accuracy at higher  $a_{11}$  with lower number of basis functions. The inset plots show the trend of  $\tilde{N}$  in the neighbourhood of  $a_{11} \approx 0$ , where there is a sharp increase.

For the limiting case of  $a_{\text{RbRb}} \rightarrow 0$ , or the non-interacting limit the Bogoliubov modes are, to a very good approximation, the eigenstates of the trapping potential. In this limit too, the condensate with the soliton has higher  $\tilde{n}$  than the condensate without soliton. An exponential increase in the total number of non-condensate atoms

$$\tilde{N} = \int_{-\infty}^{\infty} \tilde{n} dz, \quad (18)$$

is observed as  $a_{\text{RbRb}}$  is increased from near-zero to  $a_{\text{RbRb}} \approx a_0$ , this is evident from the inset plot in Fig. 2. However,  $\tilde{N}$  increases linearly with further increase of  $a_{\text{RbRb}}$  and this is shown in the main plot of Fig. 2. An important observation is that,  $d\tilde{N}/da_{\text{RbRb}} \propto N$  (total number of atoms), which is due to higher repulsive interaction energy with increasing  $N$ . This is visible in the family of curves given for different values of  $N$  in Fig. 2. It should be emphasized here that an optimal choice of basis size  $N_b$  is necessary in all the computations to obtain accurate mode functions and energies. For weakly interacting condensates with soliton, a basis set consisting of 170 basis functions give converged and reliable results. But, for the strongly interacting case  $1 \ll NU$ , the energy eigenvalues  $E_j$ s do not converge and  $\tilde{N}$  diverges as shown by the red solid line in Fig. 2 for  $N = 2000$ . However, we get converged and reliable results when the basis size is increased to 240 basis functions.

The results that we have presented in this section correspond to a condensate with a soliton at the center of the trap consisting of  $N = 2000$   $^{87}\text{Rb}$  atoms whose  $s$ -wave scattering length is  $a_{11} = a_{\text{RbRb}} = 100a_0$ , where  $a_0$  is the Bohr radius. The evolution of the low-lying modes are computed for the above-mentioned  $a_{\text{RbRb}}$  with  $\omega_z = 2\pi \times 4.55\text{Hz}$ , and  $\omega_{\perp} = 20\omega_z$ . This choice of parameters are consistent with the experimental setting and satisfies the condition of quasi-1D approximation [17, 57, 58]. It must be mentioned here that, we get almost identical results using either the harmonic oscillator basis or the *Hartree-Fock* basis. With the latter, in general, we require a smaller basis size. However, for the present work on quasi-1D condensates, the dimension of the BdG matrix is within manageable limits even with the harmonic oscillator basis.

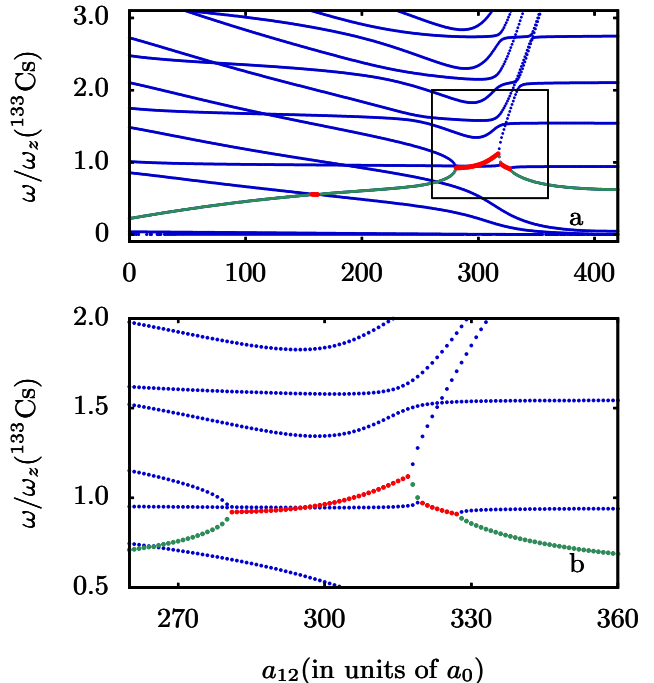


FIG. 3. The evolution of the modes as a function of the interspecies scattering length  $a_{\text{CsRb}}$  in the Rb-Cs TBEC with soliton. (a) The evolution of the low-lying modes in the domain  $0 \leq a_{\text{CsRb}} \leq 420a_0$  for  $N_{\text{Rb}} = N_{\text{Cs}} = 10^3$ . (b) The enlarged view of the region enclosed within the black colored rectangular box in (a) to resolve the mode collisions and bifurcations. The plots show only the real part of mode energies  $\omega/\omega_z$ .

### C. Interaction induced instability in TBEC

Dark solitons in one of the components in quasi-1D TBECs, like in single species, are also dynamically unstable at  $T = 0$  due to the quantum fluctuations. There is, however, another type of instability associated with dark solitons, and unique to TBECs. It arises from the

interspecies interactions, and occurs when an anomalous mode collides with a higher energy mode. The collision transforms the two modes into degenerate complex energy modes, and render the dark solitonic state unstable. In the present work, we examine the collision of the modes as a function of the interspecies scattering length, and study in detail the nature of these modes, and their evolution. Mode collisions of similar nature, giving rise to *oscillatory unstable* states, have been investigated in the context of a single species cigar-shaped BEC with dark solitons in double-well potentials [20].

In TBECs, phase separation occurs when  $U_{12} > \sqrt{U_{11}U_{22}}$ . For the present study, we consider Cs and Rb as the first and second species, respectively. With this identification  $a_{11} = a_{\text{CsCs}} = 280a_0$  and  $a_{22} = a_{\text{RbRb}} = 100a_0$ , and arrive at the condition for phase separation  $a_{12} = a_{\text{CsRb}} > 261a_0$ , which is smaller than the background value of  $a_{\text{CsRb}} \approx 650a_0$  [59]. To investigate the mode evolution with solitons, we imprint a soliton onto the first species (Cs condensate) at  $z = 0$ . We, then, vary  $a_{\text{CsRb}}$  from miscible to immiscible regime, which is experimentally possible with the Rb-Cs Feshbach resonance [60]. The mode energies,  $E_j$ , are computed at  $T = 0$  in steps of increasing  $a_{\text{CsRb}}$  in the domain  $[0, 420a_0]$  with  $N_{\text{Rb}} = N_{\text{Cs}} = 10^3$ ,  $\omega_{z(\text{Rb})} = 2\pi \times 3.89\text{Hz}$  and  $\omega_{z(\text{Cs})} = 2\pi \times 4.55\text{Hz}$  as in Ref. [58, 61]. To make the system quasi-1D we take  $\omega_{\perp} = 30\omega_z$ . The low-lying excitation spectrum is characterized by the presence of an anomalous mode signifying the presence of soliton. The other two significant low-lying modes, which are also present in quasi-1D TBECs without soliton, are the Goldstone and Kohn modes of the two species.

When  $a_{\text{CsRb}} = 0$ , the  $U_{\text{CsRb}}$  dependent terms in Eq.(16) are zero and the spectrum of the two species are independent as the two condensates are decoupled. The clear separation between the modes of the two species is lost and mode mixing occurs when  $a_{\text{CsRb}} > 0$ . For instance, the energy of the Cs anomalous mode increases with increasing  $a_{\text{CsRb}}$ , and collides with the other modes resulting in the generation of a quartet of degenerate complex mode energies. This occurs when  $a_{\text{CsRb}}$  is in the domains  $[157a_0, 162a_0]$ ,  $[281a_0, 317a_0]$ , and  $[318a_0, 327a_0]$  marked by red dots in Fig. 3. In these domains, the low-lying energy spectrum has no anomalous mode and the system is *oscillatory unstable*. For  $162a_0 < a_{\text{CsRb}} < 281a_0$ , the anomalous mode reappears and crosses the fourth excited state at  $a_{\text{CsRb}} \approx 264a_0$ . Continuing further, as evident from Fig. 3(b), at  $a_{\text{CsRb}} \approx 327a_0$  there is a bifurcation after which the anomalous mode ceases to undergo mode collisions.

It should be emphasized here that, with the transition from miscible to immiscible regime the Kohn mode and the fourth excited modes go soft. This introduces two new Goldstone modes, including which, there are four Goldstone modes in the excitation spectrum. These features deserve detailed discussion and are given in the following sections.

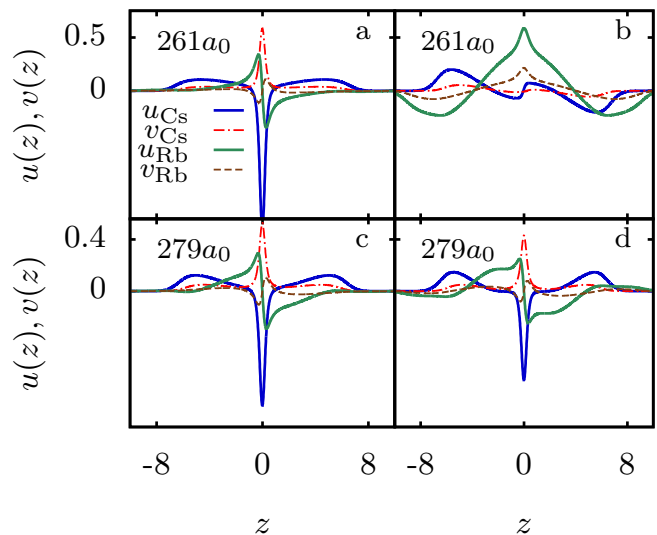


FIG. 4. Variation in the nature of mode evolution near mode crossing and collision. (a-b)Quasi-particle amplitudes corresponding to the anomalous and fourth excited mode, respectively, at  $a_{\text{CsRb}} = 261a_0$  when the modes cross each other. (c-d)Quasi-particle amplitudes corresponding to the anomalous and sixth excited mode, respectively, at  $a_{\text{CsRb}} = 279a_0$  when the modes collide. For better visibility  $u_{\text{Cs}}$  and  $u_{\text{Rb}}$  are scaled by a factor of 2.5. In the plots  $u$ 's and  $v$ 's are in units of  $a_{\text{osc}}^{-1/2}$ .

### 1. Mode collisions

From Fig. 3, it is evident that there are several instances of avoided crossings and *mode collisions* when two modes meet as  $a_{\text{CsRb}}$  is varied to higher values. We have used the latter term (mode collision) to identify the case when one of the two modes is the anomalous mode and when mode collisions do happen, the evolution of the mode energies is different from the avoided crossings. In mode collisions, there are two possible scenarios: either the two modes cross each other or undergo bifurcation. These occur due to the changes in the spatial profile of the mode functions ( $u_{\text{Rb}}$ ,  $v_{\text{Rb}}$ ,  $u_{\text{Cs}}$  and  $v_{\text{Cs}}$ ), which in turn depend on the condensate densities  $n_{ck}(z)$ .

To examine the case of two modes crossing each other during mode collision, consider the anomalous and fourth excited mode in the neighborhood of  $a_{\text{CsRb}} = 261a_0$ . At values of  $a_{\text{CsRb}}$  slightly below  $261a_0$ , the anomalous and the fourth excited mode approach and cross each other at  $a_{\text{CsRb}} \approx 261a_0$ . In this case, there are no mode mixing pre and post mode collision. As shown in Fig. 4(a), the mode functions  $u_{\text{Rb}}$  and  $v_{\text{Rb}}$  corresponding to the anomalous mode are zero at  $z = 0$ , whereas the mode functions  $u_{\text{Cs}}$  and  $v_{\text{Cs}}$ , have maxima at  $z = 0$ . In contrast, the fourth excited mode has  $u_{\text{Cs}}$  and  $v_{\text{Cs}}$  which are zero at  $z = 0$ , while  $u_{\text{Rb}}$  and  $v_{\text{Rb}}$  have maxima at  $z = 0$  as shown in Fig. 4(b). The mode functions, thus, have very different profiles at  $z = 0$  and mode mixing does not occur, instead they just cross through.

Now, let us consider the case of bifurcation at  $a_{\text{CsRb}} \approx 279a_0$ . For this value of  $a_{\text{CsRb}}$  the mode functions corresponding to the anomalous mode and the sixth mode have similar profiles with both  $u_{\text{Cs}}, v_{\text{Cs}} \neq 0$  at  $z = 0$  as shown in Fig. 4(c-d). These two modes collide and give rise to complex mode energies. A similar trend is also observed at  $a_{\text{CsRb}} \approx 157a_0$ , when the Cs anomalous mode collides with the Rb Kohn mode. In the domain  $157a_0 \leq a_{\text{CsRb}} \leq 162a_0$ , the profile of the Rb Kohn mode resembles the structure of the Cs anomalous mode. So that after mode collision, they give rise to complex eigenfrequencies and makes the states *oscillatory unstable*.

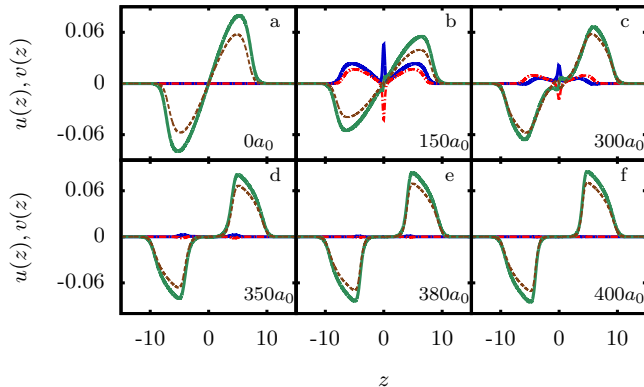


FIG. 5. Evolution of quasi-particle amplitudes corresponding to the Rb Kohn mode as  $a_{\text{CsRb}}$  is increased from 0 to  $400a_0$ . (a) At  $a_{\text{CsRb}} = 0$ , it is a Kohn mode of the Rb condensate. (b-d) In the domain  $0 < a_{\text{CsRb}} \lesssim 350a_0$  the mode acquires admixtures from the Cs Kohn mode (nonzero  $u_{\text{Cs}}$  and  $v_{\text{Cs}}$ ). (e-f) At phase separation  $310a_0 \lesssim a_{\text{CsRb}}$  the mode transforms to a Goldstone mode:  $u_{\text{Rb}}$  and  $v_{\text{Rb}}$  resemble the profile of  $n_{\text{Rb}} = |\phi_{\text{Rb}}|^2$  but with a phase difference. In the plots  $u$ 's and  $v$ 's are in units of  $a_{\text{osc}}^{-1/2}$ .

## 2. Third and fourth Goldstone modes

The third Goldstone mode emerges in the excitation spectrum as  $a_{\text{CsRb}}$  is increased, and the Rb Kohn mode goes soft at phase separation when  $a_{\text{CsRb}} \approx 350a_0$ . This is consistent with the results reported in our earlier work [45]. The evolution of the Rb Kohn mode functions ( $u_{\text{Rb}}$  and  $v_{\text{Rb}}$ ) with  $a_{\text{CsRb}}$  are shown in Fig. 5. It is evident that when  $a_{\text{CsRb}} = 0$  (Fig. 5(a)), there is no admixture from the Cs Kohn mode ( $u_{\text{Cs}} = v_{\text{Cs}} = 0$ ). However, when  $0 < a_{\text{CsRb}} \lesssim 400a_0$  the admixture from the Cs Kohn mode increases initially, and decreases to zero as we approach  $U_{\text{CsRb}} > \sqrt{U_{\text{CsCs}}U_{\text{RbRb}}}$  (Fig. 5(b-f)). So, the third Goldstone mode is present in the system when  $a_{\text{CsRb}} \gtrsim 350a_0$ .

The fourth excited mode, unlike in the case of quasi-1D TBECs without a soliton also goes soft at  $a_{\text{CsRb}} \approx 380a_0$ . The evolution of the mode functions ( $u_{\text{Rb}}$  and  $v_{\text{Rb}}$ ) corresponding to the fourth excited mode with  $a_{\text{CsRb}}$  are shown in Fig. 6. It is noticeable that when  $a_{\text{CsRb}} = 0$  (Fig.

6(a)), there is no contribution from higher energy modes of Cs. However, when  $0 < a_{\text{CsRb}}$  the admixture from the third excited mode of the Cs condensate is discernible in the lower values of  $a_{\text{CsRb}}$  and are shown in Fig. 6(b-c). At higher values of  $a_{\text{CsRb}}$ ,  $261a_0 \lesssim a_{\text{CsRb}} \lesssim 400a_0$ , the spatial profile of the mode functions are different from those of the lower values of  $a_{\text{CsRb}}$ , and are shown in Fig. 5(d-f). At around  $a_{\text{CsRb}} \approx 300a_0$ , the mode functions begin to resemble the structure of  $\phi_{\text{Rb}}$ , and the transformation is complete at  $a_{\text{CsRb}} \approx 380a_0$  when the mode goes soft.

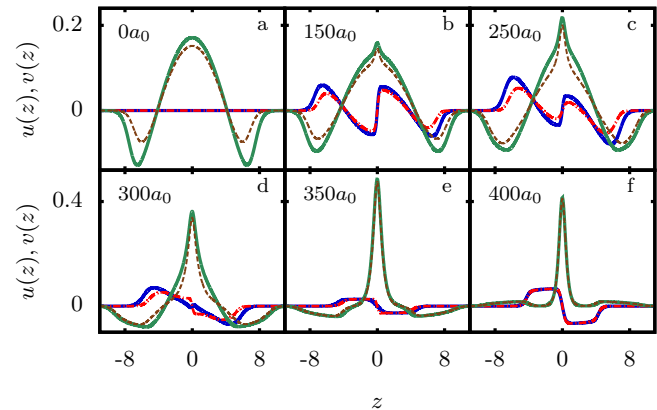


FIG. 6. Evolution of the quasi-particle amplitudes corresponding to the fourth excited mode as  $a_{\text{CsRb}}$  is increased from 0 to  $420a_0$ . (a) At  $a_{\text{CsRb}} = 0$ , it is the second excited mode of the Rb condensate. (b-d) In the domain  $0 < a_{\text{CsRb}} \lesssim 300a_0$  the mode acquires admixtures from the Cs Kohn mode (nonzero  $u_{\text{Cs}}$  and  $v_{\text{Cs}}$ ). (e-f) At phase separation  $380a_0 \lesssim a_{\text{CsRb}}$  the mode transforms to a Goldstone mode:  $u_{\text{Rb}}, v_{\text{Rb}}$  and  $u_{\text{Cs}}, v_{\text{Cs}}$  resemble the profile of  $n_{\text{Rb}} = |\phi_{\text{Rb}}|^2$  and  $n_{\text{Cs}} = |\phi_{\text{Cs}}|^2$  but with a phase difference. In the plots  $u$ 's and  $v$ 's are in units of  $a_{\text{osc}}^{-1/2}$ .

## D. Different mass ratios

To gain insight on the complex nature of the mode evolution in the Rb-Cs TBEC, we study the interplay of mass difference and intra-species scattering lengths. For the set of aforementioned parameters the ground state of TBEC, after phase separation is of *sandwich* geometry, in which the species with the heavier mass (Cs) is at the center and flanked by the species with lighter mass (Rb) at the edges [61], albeit  $a_{\text{CsCs}} \gg a_{\text{RbRb}}$ . This geometry minimizes the trapping potential energy, and hence the total energy of the system. In contrast, for TBECs with  $m_1 \approx m_2$ , at phase separation, the species with the smaller intraspecies scattering length is surrounded by the other species. In this case the mode evolution in the presence of soliton is devoid of any *mode collisions*. Thus, we attribute the pattern of mode collisions in Rb-Cs TBEC binary condensate with soliton to the interplay between mass difference and intra-species scattering lengths.

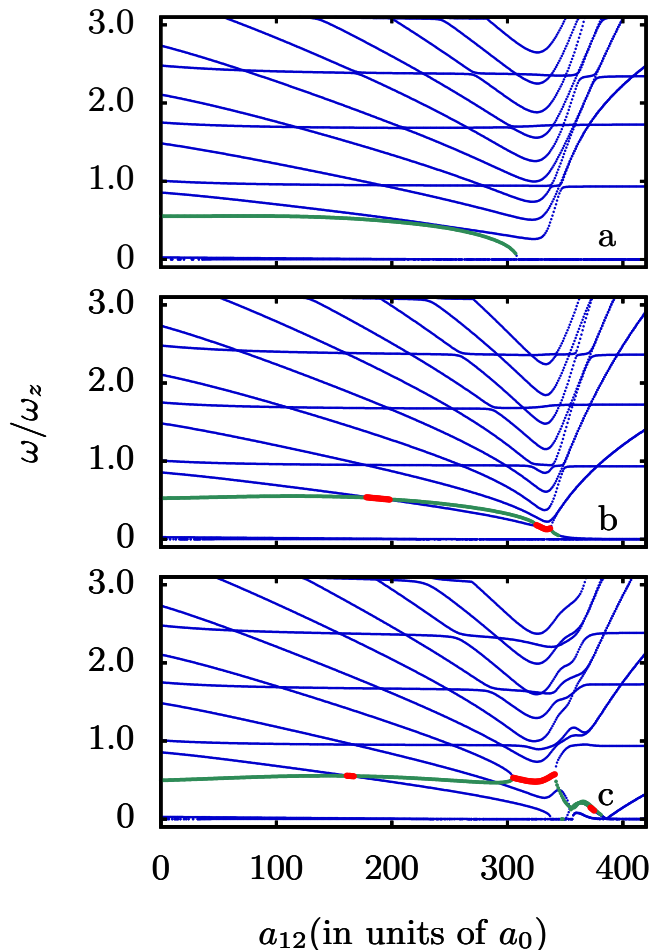


FIG. 7. The evolution of the low-lying modes of the TBEC with soliton for different mass ratios as a function of the interspecies scattering length  $a_{12}$  in the domain  $0 \leq a_{12} \leq 420a_0$ . The masses of the first and second species in each of the panels correspond to (a) 95 and 87, (b) 100 and 87, and (c) 105 and 87 amu, respectively. The number of atoms in each species is  $10^3$ . The intra-species scattering lengths of the first and second species are  $a_{11} = 280a_0$  and  $a_{22} = 100a_0$ , respectively. The plots show only the real part of mode energies  $\omega/\omega_z$ .

To understand the transition in the mode evolution from  $m_1 \approx m_2$  to a case similar to Rb-Cs TBEC, we consider a test case where  $87 \text{ amu} \leq m_1 \leq 125 \text{ amu}$  and fix  $m_2 = m_{\text{Rb}}$ . We then compute the evolution of the modes as a function of the inter-species scattering length as we increase  $m_1$  from 87 amu to 125 amu in steps of 2 amu. For example, the mode evolution for three different values of  $m_1$  (95 amu, 100 amu, and 105 amu) are shown in Fig. 7. From Fig. 7(a) it is evident that at  $m_1 = 95$  amu the anomalous mode goes soft at phase separation and becomes the third Goldstone mode of the system without any mode collisions. At  $a_{12} \approx 300a_0$ , the two species are partially miscible and the notch of  $n_1$  at  $z = 0$  due to the soliton is filled with the second species. For higher values of  $a_{12} \approx 340a_0$ , the energetically favorable state is of a *sandwich geometry* where the species with

the heavier mass ( $m_1 = 95$  amu) is at the edge of the trap and the species with lower mass ( $m_2 = 87$  amu) occupies the center. It should, however be recalled here that  $a_{11} > a_{22}$ .

There is a major change in the nature of mode evolution, as shown in Fig. 7(b) for  $m_1 = 100$ : the anomalous mode collides with the second excited mode twice at  $a_{12} \approx 180a_0$  and  $320a_0$ . The emergence of a bifurcation is evident in the second mode collision at  $a_{12} \approx 320a_0$ . On further increase of  $m_1$ , as shown in Fig. 7(c) for  $m_1 = 105$ , the trend of the mode collision begins to resemble that of the Rb-Cs mixture. In this case, the bifurcation arising from the collision between the anomalous and sixth excited mode is quite evident. Coming to the topology of the density profiles, prior to phase separation ( $a_{12} \approx 300a_0$ )  $n_1$  and  $n_2$  overlap with each other and the notch of the soliton is filled by the second species. At still higher values of  $a_{12}$ ,  $n_2$  from the edges migrates towards the notch of the soliton and the soliton gets topologically deformed. This is the energetically favorable density configuration. At  $a_{12} \approx 380a_0$ , the migration is complete and  $n_2$  occupies the center of the trap and is surrounded by  $n_1$  and the system is then phase-separated. Here, it must be mentioned that without soliton the density profile would be opposite: condensates with masses  $m_1$  and  $m_2$  occupy the center and edges, respectively. Thus, the presence of the soliton induces a change in the topology of the density profiles in TBECs. On further increase of  $m_1$ , the energy of the anomalous mode increases with increasing  $a_{12}$  and the collision with the sixth mode occurs at higher energies.

## V. CONCLUSIONS

In conclusion, we have examined the stability of solitons in single and two-component BEC. We have predicted that at zero temperature presence of soliton enhances the quantum depletion and fills up the notch of the soliton which makes it oscillatory unstable. In TBECs having a dark soliton with strong interspecies interaction, four Goldstone modes emerge in the excitation spectrum. We have also predicted that the TBECs with soliton in one of the components oscillate while interacting even at zero temperature. This is due to the non-zero density of the other species within the notch of the dark soliton. We have also shown a soliton induced change in the density profiles when the atomic masses of the two species differ widely. Based on a series of computations, we find an enhancement in the mass ratio at which the heavier species, with higher scattering length, occupies the central position at phase separation.

## ACKNOWLEDGMENTS

We thank K. Suthar, S. Chattopadhyay and S. Gautam for useful discussions. The results presented in the

paper are based on the computations using the 3TFLOP HPC Cluster at Physical Research Laboratory, Ahmed-

abad, India. We also thank the anonymous referee for the thorough review and valuable comments, which contributed to improving the quality of the manuscript.

- 
- [1] W. H. Zurek, *Nature* **317**, 505 (1985).
- [2] W. H. Zurek, *Phys. Rev. Lett.* **102**, 105702 (2009).
- [3] B. Damski and W. H. Zurek, *Phys. Rev. Lett.* **104**, 160404 (2010).
- [4] G. Lamporesi, S. Donadello, S. Serafini, F. Dalfovo, and G. Ferrari, *Nat. Phys.* **9**, 656 (2013).
- [5] A. Negretti and C. Henkel, *J. Phys. B* **37**, L385 (2004).
- [6] A. Negretti, C. Henkel, and K. Mølmer, *Phys. Rev. A* **78**, 023630 (2008).
- [7] S. Burger, K. Bongs, S. Dettmer, W. Ertmer, K. Sengstock, A. Sanpera, G. V. Shlyapnikov, and M. Lewenstein, *Phys. Rev. Lett.* **83**, 5198 (1999).
- [8] J. Denschlag, J. E. Simsarian, D. L. Feder, C. W. Clark, L. A. Collins, J. Cubizolles, L. Deng, E. W. Hagley, K. Helmerson, W. P. Reinhardt, S. L. Rolston, B. I. Schneider, and W. D. Phillips, *Science* **287**, 97 (2000).
- [9] T. Busch and J. R. Anglin, *Phys. Rev. Lett.* **84**, 2298 (2000).
- [10] T. Busch and J. R. Anglin, *Phys. Rev. Lett.* **87**, 010401 (2001).
- [11] S. Middelkamp, J. Chang, C. Hamner, R. Carretero-González, P. Kevrekidis, V. Achilleos, D. Frantzeskakis, P. Schmelcher, and P. Engels, *Phys. Lett. A* **375**, 642 (2011).
- [12] M. A. Hoefler, J. J. Chang, C. Hamner, and P. Engels, *Phys. Rev. A* **84**, 041605 (2011).
- [13] K. Kasamatsu and M. Tsubota, *Phys. Rev. A* **74**, 013617 (2006).
- [14] S. Rajendran, P. Muruganandam, and M. Lakshmanan, *J. Phys. B* **42**, 145307 (2009).
- [15] V. Achilleos, D. Yan, P. G. Kevrekidis, and D. J. Frantzeskakis, *New Journal of Physics* **14**, 055006 (2012).
- [16] C. Becker, S. Stellmer, P. Soltan-Panahi, S. Dörscher, M. Baumert, E.-M. Richter, J. Kronjäger, K. Bongs, and K. Sengstock, *Nat. Phys.* **4**, 496 (2008).
- [17] A. Weller, J. P. Ronzheimer, C. Gross, J. Esteve, M. K. Oberthaler, D. J. Frantzeskakis, G. Theoharis, and P. G. Kevrekidis, *Phys. Rev. Lett.* **101**, 130401 (2008).
- [18] S. Stellmer, C. Becker, P. Soltan-Panahi, E.-M. Richter, S. Dörscher, M. Baumert, J. Kronjäger, K. Bongs, and K. Sengstock, *Phys. Rev. Lett.* **101**, 120406 (2008).
- [19] A. E. Muryshev, H. B. van Linden van den Heuvell, and G. V. Shlyapnikov, *Phys. Rev. A* **60**, R2665 (1999).
- [20] S. Middelkamp, G. Theoharis, P. G. Kevrekidis, D. J. Frantzeskakis, and P. Schmelcher, *Phys. Rev. A* **81**, 053618 (2010).
- [21] M. Mochol, M. Płodzień, and K. Sacha, *Phys. Rev. A* **85**, 023627 (2012).
- [22] P. G. Kevrekidis, R. Carretero-González, G. Theoharis, D. J. Frantzeskakis, and B. A. Malomed, *Phys. Rev. A* **68**, 035602 (2003).
- [23] N. G. Parker, N. P. Proukakis, C. F. Barenghi, and C. S. Adams, *J. Phys. B* **37**, S175 (2004).
- [24] H. Sakaguchi and B. A. Malomed, *Phys. Rev. E* **72**, 046610 (2005).
- [25] Y. V. Kartashov, B. A. Malomed, and L. Torner, *Rev. Mod. Phys.* **83**, 247 (2011).
- [26] R. Atre, P. K. Panigrahi, and G. S. Agarwal, *Phys. Rev. E* **73**, 056611 (2006).
- [27] G. Theoharis, A. Weller, J. P. Ronzheimer, C. Gross, M. K. Oberthaler, P. G. Kevrekidis, and D. J. Frantzeskakis, *Phys. Rev. A* **81**, 063604 (2010).
- [28] J. Dziarmaga and K. Sacha, *Phys. Rev. A* **66**, 043620 (2002).
- [29] J. Dziarmaga, Z. P. Karkuszewski, and K. Sacha, *Phys. Rev. A* **66**, 043615 (2002).
- [30] J. Dziarmaga and K. Sacha, *Phys. Rev. A* **67**, 033608 (2003).
- [31] J. Dziarmaga, Z. P. Karkuszewski, and K. Sacha, *J. Phys. B* **36**, 1217 (2003).
- [32] C. K. Law, P. T. Leung, and M.-C. Chu, *J. Phys. B* **35**, 3583 (2002).
- [33] C. K. Law, *Phys. Rev. A* **68**, 015602 (2003).
- [34] D. M. Gangardt and A. Kamenev, *Phys. Rev. Lett.* **104**, 190402 (2010).
- [35] S. B. Papp, J. M. Pino, and C. E. Wieman, *Phys. Rev. Lett.* **101**, 040402 (2008).
- [36] S. Tojo, Y. Taguchi, Y. Masuyama, T. Hayashi, H. Saito, and T. Hirano, *Phys. Rev. A* **82**, 033609 (2010).
- [37] T.-L. Ho and V. B. Shenoy, *Phys. Rev. Lett.* **77**, 3276 (1996).
- [38] S. Gautam and D. Angom, *J. Phys. B* **43**, 095302 (2010).
- [39] S. Gautam and D. Angom, *J. Phys. B* **44**, 025302 (2011).
- [40] K. Sasaki, N. Suzuki, D. Akamatsu, and H. Saito, *Phys. Rev. A* **80**, 063611 (2009).
- [41] S. Gautam and D. Angom, *Phys. Rev. A* **81**, 053616 (2010).
- [42] T. Kadokura, T. Aioi, K. Sasaki, T. Kishimoto, and H. Saito, *Phys. Rev. A* **85**, 013602 (2012).
- [43] H. Takeuchi and K. Kasamatsu, *Phys. Rev. A* **88**, 043612 (2013).
- [44] C. Ticknor, *Phys. Rev. A* **88**, 013623 (2013).
- [45] A. Roy, S. Gautam, and D. Angom, *Phys. Rev. A* **89**, 013617 (2014).
- [46] C. Ticknor, *Phys. Rev. A* **89**, 053601 (2014).
- [47] P. Mason and S. A. Gardiner, *Phys. Rev. A* **89**, 043617 (2014).
- [48] C. Hamner, J. J. Chang, P. Engels, and M. A. Hoefler, *Phys. Rev. Lett.* **106**, 065302 (2011).
- [49] P. Öhberg and L. Santos, *J. Phys. B* **34**, 4721 (2001).
- [50] P. Öhberg and L. Santos, *Phys. Rev. Lett.* **86**, 2918 (2001).
- [51] P. G. Kevrekidis, H. E. Nistazakis, D. J. Frantzeskakis, B. A. Malomed, and R. Carretero-González, *Eur. Phys. J. D* **28**, 181 (2004).
- [52] D. Schumayer and B. Apagyí, *Phys. Rev. A* **69**, 043620 (2004).
- [53] R. J. Dodd, M. Edwards, C. W. Clark, and K. Burnett, *Phys. Rev. A* **57**, R32 (1998).
- [54] A. Griffin, *Phys. Rev. B* **53**, 9341 (1996).

- [55] P. Muruganandam and S. K. Adhikari, *Comp. Phys. Comm.* **180**, 1888 (2009).
- [56] E. Anderson, Z. Bai, C. Bischof, S. Blackford, J. Demmel, J. Dongarra, J. D. Croz, A. Greenbaum, S. Hammarling, A. McKenney, and D. Sorensen, *LAPACK Users' Guide*, 3rd ed. (Society for Industrial and Applied Mathematics, Philadelphia, PA, 1999).
- [57] A. Görlitz, J. M. Vogels, A. E. Leanhardt, C. Raman, T. L. Gustavson, J. R. Abo-Shaeer, A. P. Chikkatur, S. Gupta, S. Inouye, T. Rosenband, and W. Ketterle, *Phys. Rev. Lett.* **87**, 130402 (2001).
- [58] R. W. Pattinson, T. P. Billam, S. A. Gardiner, D. J. McCarron, H. W. Cho, S. L. Cornish, N. G. Parker, and N. P. Proukakis, *Phys. Rev. A* **87**, 013625 (2013).
- [59] A. Lercher, T. Takekoshi, M. Debatin, B. Schuster, R. Rameshan, F. Ferlaino, R. Grimm, and H.-C. Ngerl, *Euro. Phys. Jour. D* **65**, 3 (2011).
- [60] K. Pilch, A. D. Lange, A. Prantner, G. Kerner, F. Ferlaino, H.-C. Nägerl, and R. Grimm, *Phys. Rev. A* **79**, 042718 (2009).
- [61] D. J. McCarron, H. W. Cho, D. L. Jenkin, M. P. Köppinger, and S. L. Cornish, *Phys. Rev. A* **84**, 011603 (2011).